Int J Adv Manuf Technol (2013) 65:259–274
DOI 10.1007/s00170-012-4165-5

ORIGINAL ARTICLE

An integrated evolutionary approach for modelling and optimization of laser beam cutting process

D. Kondayya · A. Gopala Krishna

Received: 25 May 2011 / Accepted: 10 April 2012 / Published online: 8 May 2012

Abstract This paper presents a new integrated methodology based on evolutionary algorithms (EAs) to model and optimize the laser beam cutting process. The proposed study is divided into two parts. Firstly, genetic programming (GP) approach is used for empirical modelling of kerf width (Kw) and material removal rate (MRR) which are the important performance measures of the laser beam cutting process. GP, being an extension of the more familiar genetic algorithms, recently has evolved as a powerful optimization tool for nonlinear modelling resulting in credible and accurate models. Design of experiments is used to conduct the experiments. Four prominent variables such as pulse frequency, pulse width, cutting speed and pulse energy are taken into consideration. The developed models are used to study the effect of laser cutting parameters on the chosen process performances. As the output parameters Kw and MRR are mutually conflicting in nature, in the second part of the study, they are simultaneously optimized by using a multi-objective evolutionary algorithm called non-dominated sorting genetic algorithm II. The Pareto optimal solutions of parameter settings have been reported that provide the decision maker an elaborate picture for making the optimal decisions. The work presents a full-fledged evolutionary approach for optimization of the process.

D. Kondayya (✉)
Department of Mechanical Engineering,
Sreenidhi Institute of Science and Technology,
Hyderabad PIN-501 301 Andhra Pradesh, India
e-mail: d_kondayya@yahoo.co.in

A. Gopala Krishna
Department of Mechanical Engineering, University College of Engineering, Jawaharlal Nehru Technological University,
Kakinada PIN-533 003 Andhra Pradesh, India
e-mail: dr.a.gopalakrishna@gmail.com

Keywords Laser beam cutting · Modelling · Genetic programming · Multi-objective optimization · NSGA-II

1 Introduction

Laser beam cutting belongs to the group of thermal cutting processes wherein the output of high-power laser is directed and focused to a small spot on the material to be cut. The material then either melts or vaporizes. As the beam moves relative to the material, a cut channel (the kerf) is formed, having an edge with a high-quality surface finish. The molten material is blown out of the developing kerf by using a relatively high-pressure coaxial assist gas. The principle of laser beam cutting is shown in Fig. 1. Of all the industrial laser cutting applications, the vast majority of these are used for the cutting of metal sheets worldwide and this application has progressed dramatically in the past 5 years [1]. The reasons for the widespread usage of lasers for cutting of metallic sheets is: process is fast and noncontact, superior edge quality, low surface roughness, small heat-affected zones (HAZ), ability to create fine and intricate details [2].

The most important performance measures in laser cutting are kerf width (Kw) and material removal rate (MRR) [3]. Kerf width indicates the degree of accuracy, whereas material removal rate decides the production rate and economics of machining. These performance measures are affected by input cutting variables such as laser power, pulse frequency, pulse duration, type of assist gas and gas pressure. Laser cutting is a highly complicated process wherein a large number of parameters need to be precisely controlled in unison, hence experimental optimization of the process is costly and time-consuming. Moreover owing to the nonlinearity and the highly complicated interactions between process parameters of the laser process, the current analytical models cannot provide

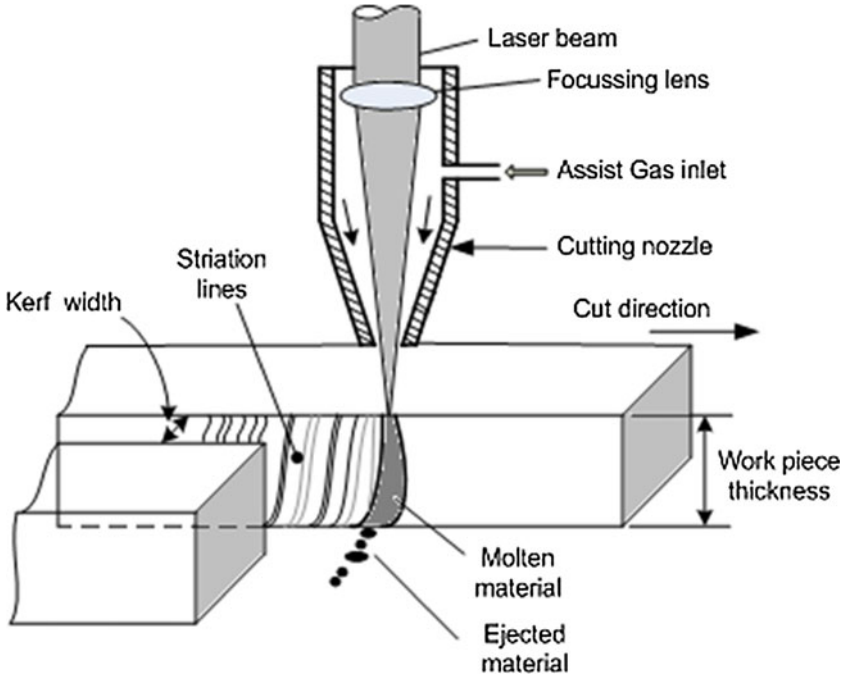

Fig. 1 Laser beam cutting process

accurate process prediction for better quality control and higher throughput. Therefore an efficient method is needed to determine the optimal parameters for best cutting performance. The performance measures as stated earlier viz. kerf width and material removal rate are conflicting in nature, as lower value of kerf width and higher value of material removal rate are preferred.

The overall objective of this research is to apply a new process modelling and optimization methodology for the highly nonlinear and complex manufacturing process of laser cutting. With this aim, accurate prediction models to estimate Kw and MRR were developed from the experimental data using a potential evolutionary modelling algorithm called genetic programming (GP). Subsequently, the developed models were used for optimization of the process. As the chosen objectives, Kw and MRR are opposite in nature, the problem was formulated as a multi-objective optimization problem. Later, a popular evolutionary algorithm, non-dominated sorting genetic algorithm II (NSGA-II), was used to retrieve the multiple optimal sets of input variables.

2 Literature review

Yousef et al. [4] have used artificial neural network (ANN) to model and analyse the nonlinear laser micro-machining process in an effort to predict the level of pulse energy needed to create a dent or crater with the desired depth and diameter on surface of a material foil. Li et al. [5] have employed Taguchi's experimental method for examining the laser cutting quality of a quad flat non-lead (QFN) package used in semiconductor packaging technology. From the study they could observe that 95.47 % of laser cutting quality is contributed from only three control factors—laser frequency, cutting speed and driving current. Experimental design and artificial neural networks have been used by Jimin et al. [6] for optimizing the parameters of 3D non-vertical laser cutting of 1-mm-thick mild steel. Dhara et al. [7] have adopted the artificial neural networks approach to optimize the machining parameter combination for the responses of depth of groove and height of recast layer in laser micro-machining of die steel. Dubey and Yadava [8] have performed the multi-response optimization of laser beam cutting process of thin sheets (0.5 mm thick) of magnetic material using hybrid Taguchi method and response surface method. The same authors [9] have performed the multi-objective optimization of kerf quality using two kerf qualities such as kerf deviation and kerf width using Taguchi quality loss function for pulsed Nd:YAG laser cutting of thin sheet of aluminium alloy. The multiple regression analysis and the artificial neural network have been applied by Ming-Jong et al. [10] to establish a predicting model for cutting 5×5 QFN packages by using a diode-pumped solid-state laser system considering current, frequency and the cutting speed as input variables and six laser cutting qualities as output variables of the QFN packages, respectively. The genetic algorithm has been finally applied to find the optimal cutting parameters leading to less HAZ width and fast cutting speed ensuing complete cutting.

Literature review infers considerable researchers conducted distinctive investigations for improving the process performance of laser cutting. In this direction empirical models establishing the relationships between the inputs and outputs were developed and these models were utilized as objective

functions and were optimized to obtain the machining conditions for the required responses. Literature review also reveals that the dominant tools for modelling and optimization used to date have been Taguchi-based regression analysis, multiple regression method, response surface methodology and ANNs.

In multiple regression and response surface methodology, a prediction model has to be determined in advance and a set of coefficients has to be found. The prespecified size and shape of the model imply that the model might not be able adequate to capture a complex relation between the influencing variables and response parameters. Like the aforementioned approaches, although ANNs have also been used extensively in the literature for modelling, they have the drawback of not being able to quantify explicitly the relationships between inputs and outputs. Though many research papers have been published on Taguchi method and ANNs as per the authors' knowledge, very limited research work has been reported pertaining to the literature on multi-objective optimization of Kw and MRR of laser beam cutting of steels. Hence, an effort has been made in this paper, which confers the application of evolutionary method for multi-objective optimization of laser cutting process.

3 Proposed methodology

In this paper, a novel approach is presented for modelling of kerf width and material removal rate using GP. The distinctive aspect of GP as compared to traditional approaches is that it does not make any presumption about the formulation to be made. Also the generated model helps directly to obtain an interpretation of the parameters affecting the process. More details of this methodology are discussed in Section 4. The models developed by GP are subsequently used for optimization.

In the current study, unlike the previous approaches, the optimization problem of laser beam cutting process is explicitly formulated as a multi-objective optimization problem, as the determination of the optimal machining conditions involves a conflict between maximizing MRR and minimizing the kerf width. It can be noted that the classical optimization methods (weighted sum methods, goal programming, min–max methods, etc.) are not efficient for handling multi-objective optimization problems because they do not find multiple solutions in a single run, and therefore, it is necessary for them to be applied as many times as the number of desired Pareto optimal solutions [11]. The above-mentioned difficulty of classical optimization methods is eliminated in evolutionary algorithms, as they can find the multiple solutions in a single run. As a result, a most commonly used evolutionary approach, the NSGA-II, is proposed in this paper for multi-objective optimization of laser beam cutting process. GA-based multi-objective optimization methodologies have been widely used in the literature to find Pareto optimal solutions. In particular, NSGA-II has proven its effectiveness and efficiency in finding well-distributed and well-converged sets of near Pareto optimal solutions [12]. The proposed methodology of integrating GP and NSGA-II is depicted in Fig. 2.

4 Modelling using GP

GP [13] is an evolutionary optimization method that emulates the concepts of natural selection and genetics and is a variant of the more familiar genetic algorithm [14]. GP's

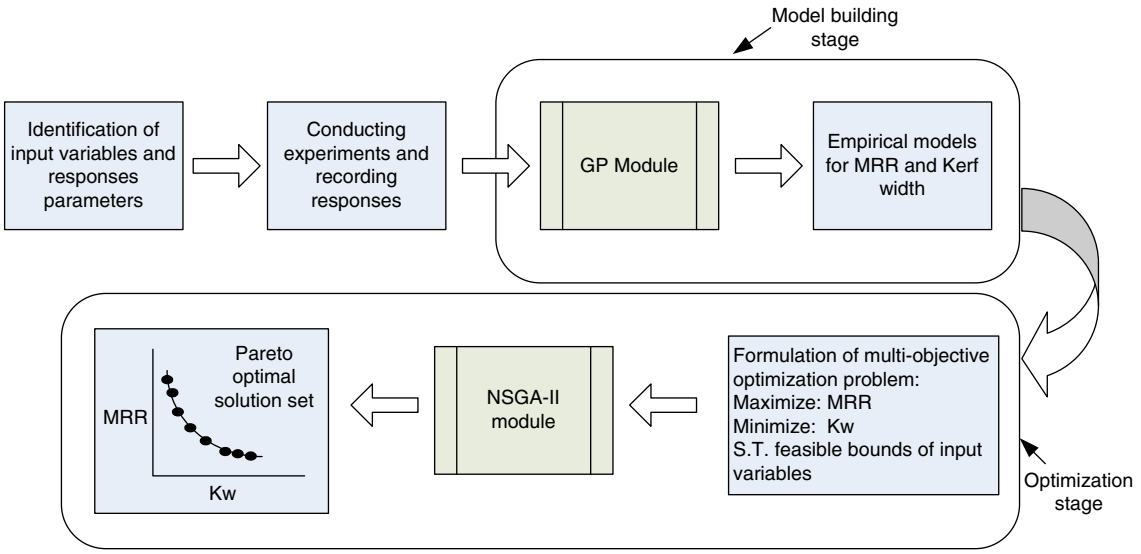

Fig. 2 Proposed methodology

ability to generate ingenious and insightful solutions has been applied actively in numerous academic and industrial research areas. Successful results have been achieved in varied problem domains such as industrial robotics [15], fault detection [16], prediction of shear strength of beams [17] and machining [18].

The first step in GP implementation is to randomly generate the initial population for a given population size. For initialization, the ramped half and half method is used widely [19] as it generates parse trees of various sizes and shapes. Also this method renders a good coverage of the search space [13]. At each generation, new sets of models are evolved by applying the genetic operators: selection, crossover and mutation. These new models are known as offspring, and they form the basis for the next generation. With each passing generation, it is presumed that the fitness of the best individual and that of the entire population will show improvement than in preceding generations. This process generally continues until an ideal individual has been found or a stipulated number of generations have been processed.

5 Optimization using NSGA-II

Among the various EAs, GAs have been the most popular heuristic and global alternative approach to multi-objective design and optimization problems [20]. These algorithms have attracted significant attention from the research community over the last two decades because of their inherent advantage in solving nonlinear objective functions. Of these, the elitist NSGA-II has received the most attention because of its lucidity and demonstrated excellence over other methods [21] for seeking Pareto optimal objective function fronts.

The various steps in NSGA-II based on the main framework of the algorithm [22] shown in Fig. 3 can be stated in the following steps:

1. Set the initial run parameters for the algorithm, viz. population size (N), maximum number of generations (g_{max}), crossover probability (P_c), mutation probability (P_m; generation, g=0).
2. Randomly create an initial population P_g of size N with a good coverage of the search space, and thereby have a diverse gene pool with potential to explore as much of the search space as possible.
3. Evaluate the objective values and rank the population using the concept of domination. Each solution is assigned a fitness (or rank) equal to its non-domination level (1 is the best level, 2 is the next best level and so on).
4. Perform the crowding sort procedure and include the most widely solutions by using crowding distance value.
5. The child populations Q_g is produced from the parent population P_g using binary selection, recombination and mutation operators.
6. Then the two populations are combined together to produce R_g (=P_g U Q_g), which is of size 2N.
7. After this the population R_g undergoes non-dominated sorting to achieve a global non-domination check.
8. The new population P_{g+1} is filled based on the ranking of the non-dominated fronts.
9. Since the combined population is twice the size of the population size N, all the fronts are not allowed to be used. Therefore a crowding distance sorting is performed in descending order and the population is filled. Thus for this new population P_{g+1}, the whole process is repeated.
10. Update the number of generations, g=g+1.
11. Repeat steps 3 to 10 until a stopping criterion is met.

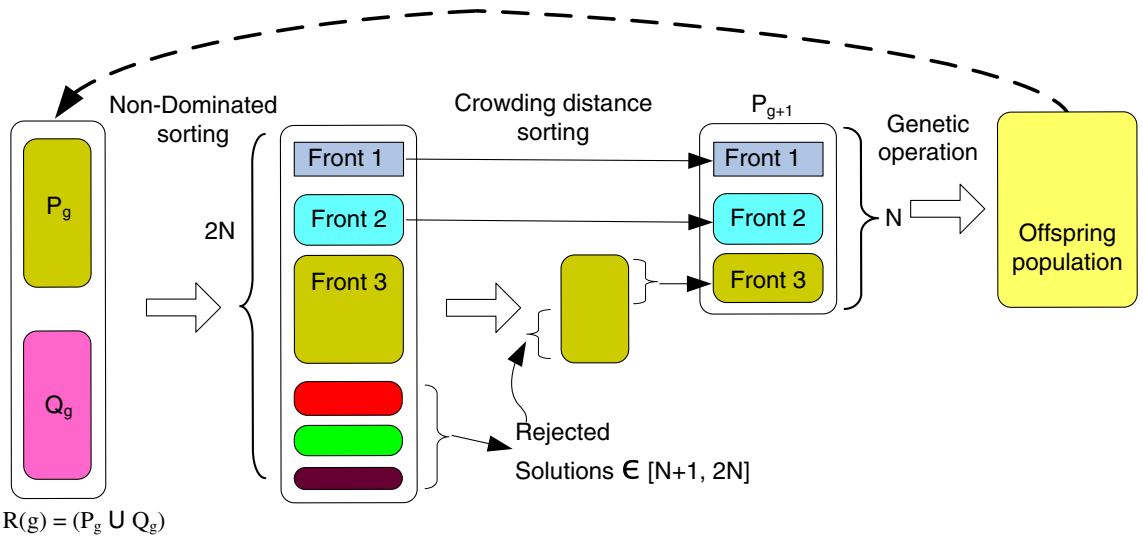

Fig. 3 Main frame work of NSGA-II algorithm

6 Experimental details

The experimentation was performed with an optical fibre delivered pulsed Nd:YAG laser beam system (Model: JK300D) manufactured by GSI Lumonics and delivering maximum peak power of 16 kW. The laser beam was transferred via a 300-μm diameter step-indexed optical fibre to the cutting head, which was mounted over a six-axis robot (Model: IRB1410) manufactured by ABB. The robot is compact in design having a weight of 225 kg, has a handling capacity of 5 kg at the wrist, has a large working area and long reach (fifth axis—1.44 m). The cutting head was fitted with an automatic standoff adjusting servomotor and electrostatic sensor. This is necessary for adapting the position and focusing the lens. The sensor is interfaced to the robot control and can read the real position of the workpiece. The robot consequently moves the lens so as to always be correctly in focus. The schematic view of robotic laser cutting system is shown in Fig. 4. The laser mode and wavelength are TEM_{00} mode and 1,064 nm. The output laser beam is focused by a BK7 plano-convex lens whose focal distance is 116 mm.

The parameters that affect the performance of the laser beam cutting process are identified based on the literature survey and preliminary investigations. Through the above exploration, four parameters which predominantly affect the material removal rate and kerf width were selected. Pulse frequency, pulse width, cutting speed and pulse energy are considered as control variables. Oxygen gas with a purity of 99.99 % was employed as an assist gas. The gas pressure was consistently maintained at 5 bar. The specimens were laser cut from AISI304L sheets of 1.70 mm thickness. The sheet material was supported firmly on a fixture to counter vibration during cutting, and the robot was programmed to traverse the cutting head in stated path. The two quality characteristics analysed are kerf width and material removal rate. The kerf width was measured with tool maker's microscope of ×10 magnification and least count of 1 μm. Kerf width of each cut was measured at three different places for accurate evaluation. The MRR is calculated by the weight loss method. The weight of the component before and after the cut was accurately measured using a digital balance which can measure up to the accuracy of 1 mg (Model XB320M, Make: Precisa).

The fixed conditions at which the experiments were conducted are listed in Table 1. Table 2 shows the different levels of the parameters used in the experimentation. The levels were fixed based on detailed preliminary experiments. The observations of the cutting process are based on second-order central composite rotatable design. The four control variables, viz. pulse frequency, pulse width, cutting speed and pulse energy each at five levels, were chosen. The results for 31 experiments after laser beam cutting which were evaluated as stated earlier on two performance measures are shown in Table 3. This table constitutes the training dataset and was used to predict the expression that best suits to the problem. Additional experiments were performed to generate the validation data. The

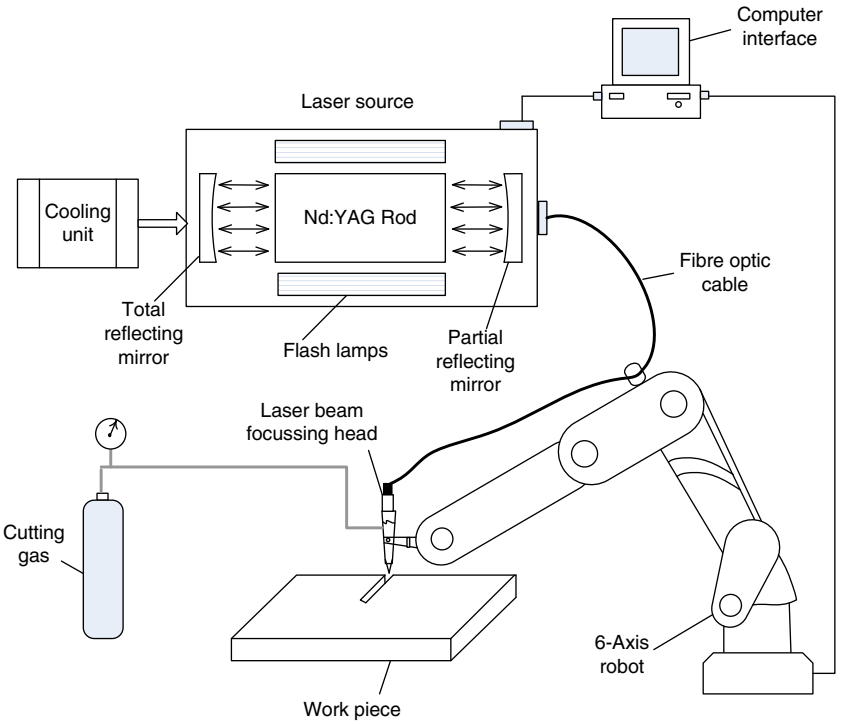

Fig. 4 Schematic of robotic laser beam cutting system

Table 1 Cutting conditions

(a) Workpiece material: AISI304L
(b) Workpiece dimensions—10 mm L × 10 mm B × 1.7 mm T
(c) Length of cut—5 mm
(d) Angle of cut: vertical
(e) Mode of operation: pulsed
(f) Nozzle diameter—1.2 mm
(g) Nozzle standoff—0.5 mm
(h) Focal lens—120 mm
(i) Focal spot size—0.1 mm
(j) Gas pressure—5 bar

validation data are utilized to validate the developed model and to ensure the generalization capability of the predicted model for unseen cases. Table 4 shows the validation dataset.

7 Implementation of GP

There are four major steps for applying genetic programming:

1. Elements of functional set and terminal set,
2. Fitness measure,
3. Parameters for controlling the run and
4. Termination criteria.

7.1 Function set and terminal set

The function set consists of standard arithmetic functions, i.e. addition (+), subtraction (−), multiplication (×) and division(/). Symbol "/" stands for protected division which merely prevents numerical overflow by division with zero. The terminal set includes the dependent variables of the laser cutting process, together with numerical real constants in the range (−100, 100).

7.2 Fitness measure

The most important concept of GP is the fitness function. The success of a problem greatly depends on the way the fitness function is designed. In this problem the fitness function used for the evolution of the GP models is the correlation coefficient R^2.

7.3 Control parameters and termination criteria

The GP algorithm requires the specification of proper set of parameters such as number of generations, population size, crossover probability, mutation probability, reproduction probability, selection method and depth of tree. Several thumb rules are given in reference [13] for parameter selection based on simulation experience for standard GP. Similar recommendations are given in Banzhaf et al. [23]. Exploration of parameters based on the guidelines was performed, and the sensitivity to certain parameters such as population size and number of generations was investigated. The value of other parameters was simply fixed reasonably. Table 5 lists the GP parameters common to both the models. The termination criteria used were the number of generations.

The choice of population size is clearly dependent on the problem being tackled, with some problems requiring thousands of population members [24]. However in the present study, population of different sizes, viz. 300, 400, 500 and 1,000, was tested upon. It was found that the use of larger population size gave more accurate model prediction but resulted in much complex models which are difficult to interpret and comprehend. Thus a population size of 300 was decided upon. The number of generations was fixed to 50 as no significant improvement was observed beyond that number. This initial randomized population is created using ramped half and half tree generation strategy, which generates a set of random trees having a variety of sizes and shapes. Half the trees are grow trees, in which each randomly generated node has an equal chance of being function (internal node) or terminal (leaf), up to a maximum depth for the tree. The other trees are full trees, where nodes are leaf nodes only when the maximum depth of the tree has been reached. Ramped tree generation proceeds until the population is filled. Crossover is performed on 85 % of the population. In addition, fitness proportionate reproduction is performed on 10 % of the population on each generation.

Table 2 LBC parameters and their level used in experimentation

Process parameter	Notation	Level 1	Level 2	Level 3	Level 4	Level 5
Pulse frequency (Hz)	x_1	51	113.25	175.5	237.75	300.27
Pulse width(ms)	x_2	0.20	0.40	0.60	0.80	1.0
Cutting speed (mm/min)	x_3	400	550	700	850	1,000
Pulse energy (J)	x_4	0.93	2.14	3.35	4.56	5.78

Table 3 Training dataset

Experiment number	x_1 (Hz)	x_2 (ms)	x_3 (mm/min)	x_4 (J)	Kw (mm)	MRR (g/min)
1	113.25	0.4	550	2.14	0.328	3.210
2	113.25	0.8	550	2.14	0.330	2.992
3	237.75	0.4	550	2.14	0.341	3.345
4	237.75	0.8	550	2.14	0.350	3.361
5	113.25	0.4	850	2.14	0.320	3.074
6	113.25	0.8	850	2.14	0.315	3.163
7	237.75	0.4	850	2.14	0.330	3.203
8	237.75	0.8	850	2.14	0.335	3.210
9	113.25	0.4	550	4.56	0.428	3.860
10	113.25	0.8	550	4.56	0.410	3.680
11	237.75	0.4	550	4.56	0.428	3.967
12	237.75	0.8	550	4.56	0.398	3.774
13	113.25	0.4	850	4.56	0.398	3.667
14	113.25	0.8	850	4.56	0.413	3.850
15	237.75	0.4	850	4.56	0.419	3.830
16	237.75	0.8	850	4.56	0.368	3.855
17	175.5	0.2	700	3.35	0.367	3.522
18	175.5	1.0	700	3.35	0.361	3.328
19	51	0.6	700	3.35	0.350	3.185
20	300	0.6	700	3.35	0.365	3.375
21	175.5	0.6	400	3.35	0.363	3.600
22	175.5	0.6	1,000	3.35	0.375	3.550
23	175.5	0.6	700	0.93	0.287	2.835
24	175.5	0.6	700	5.78	0.483	4.265
25	175.5	0.6	700	3.35	0.384	3.547
26	175.5	0.6	700	3.35	0.375	3.560
27	175.5	0.6	700	3.35	0.380	3.508
28	175.5	0.6	700	3.35	0.381	3.519
29	175.5	0.6	700	3.35	0.379	3.600
30	175.5	0.6	700	3.35	0.369	3.503
31	175.5	0.6	700	3.35	0.370	3.513

Although Koza [13] did not use the mutation, it was thought that their inclusion would be more beneficial in this study due to the relatively small population sizes used.

GP is stochastic by nature, and hence, the results will vary from one run to the next. It is standard practice for the experimenter to perform multiple independent training runs of fixed number of generations each and then report the results of the fittest individual evolved across all runs. After 50 generations and of all runs, the final selected model expression for kerf width and material removal rate having best fitness (i.e. highest R^2 value) are given hereunder:

$$\mathrm{Kw} = \frac{(28.07 + x_4) - \left(\frac{x_3(0.09x_4 - x_2 + 29.38)}{(4.40 + 242x_3 - x_2x_3)}\right)}{(92 - x_4) + \left(\frac{23(x_2 - x_4)}{8.95 - x_2}\right) - \left(\frac{0.38}{x_1x_4}\right)} \tag{1}$$

$$\mathrm{MRR} = \left(3 + 0.239(x_4 - x_2) + \frac{x_4}{x_1}\right) - \left(0.01x_3 - \frac{39}{x_1}\right) \times \left(\frac{5(19x_2 + 1604.17)}{(x_3 - 95(x_4 - x_1))(16 + x_4)}\right) \tag{2}$$

It should be noted that the proposed models are valid between the range of the input variables as given in Table 2. The convergence curves showing the progress of GP run for kerf width and MRR are given in Figs. 5 and 6. The algorithm evolves towards improving the R^2 value of the model with each generation. The values of the correlation coefficient at the end of the generation for Kw and MRR are 0.999 and 0.998. This indicates

Table 4 Validation dataset

Experiment number	x_1 (Hz)	x_2 (ms)	x_3 (mm/min)	x_4 (J)	Kw (mm)	MRR (g/min)
1	60	0.25	425	1.20	0.35	3.41
2	60	0.45	545	2.20	0.33	3.45
3	100	0.65	665	3.20	0.39	3.20
4	100	0.85	785	4.20	0.38	3.90
5	140	1.00	910	5.20	0.45	4.21
6	140	0.25	425	1.20	0.31	3.50
7	180	0.25	545	2.20	0.35	3.49
8	180	0.45	665	3.20	0.39	3.65
9	220	0.65	785	4.20	0.39	3.99
10	220	0.85	910	5.20	0.45	4.10
11	100	1.00	425	1.20	0.33	3.22
12	140	0.25	545	2.20	0.35	3.49
13	180	0.45	665	3.20	0.36	3.69
14	220	0.65	785	4.20	0.41	3.99
15	140	0.85	910	5.20	0.42	4.02

that the GP model has been able to learn the complex relationship between the input and output parameters with a good accuracy.

The normal probability plot of residuals for Kw and MRR are shown in Figs. 7 and 8. These plots reveal that the residuals are established on a straight line clearly indicating that the normal distribution of the errors and the obtained models are reasonably acceptable. The performance comparison of the trained GP model using the validation datasets for Kw and MRR are shown in Figs. 9 and 10. The high values of R^2 obtained for both the outputs indicate the models have acquired sufficient level of generalization without overfitting.

In order to have an idea about the predictive power of GP in comparison to response surface methodology (RSM), regression analysis is carried out using the same experimental dataset as used for generating GP models. The following second-order regression models were determined for kerf width and material removal rate.

$$\mathrm{Kw} = 0.037 + 0.001x_1 + 0.21x_2 + 0.058x_4 - 0.077x_2^2 + 0.001x_4^2 - 0.024x_2x_4 \quad (3)$$

$$\mathrm{MRR} = 2.895 + 0.008x_1 - 0.748x_2 - 0.002x_3 + 0.229x_4 - 0.502x_2^2 + 0.007x_4^2 + 0.001x_2x_3 - 0.015x_2x_4 \quad (4)$$

Table 6 shows the summarized error statistics for the two modelling methods. From the table it can be observed that GP has produced more accurate models than RSM.

Table 5 GP control parameters

Terminal set	$\{x_1, x_2, x_3, x_4\}$
Function set	$\{+, -, \times, \div\}$
Population size	300
Number of generations (maximum)	50
Number of independent runs	10
Crossover probability (%)	85
Mutation probability (%)	5
Reproduction probability (%)	10
Selection method	Tournament
Fitness measure	R^2
Maximum depth of tree	6

7.4 Interpretation of developed models

The evolved equations indicate some distinct aspects of GP. The final model form clearly indicates the relative contribution of each input to the output. Also the explicit relation allows simple impromptu interpretation of the problem at hand. For example, in Eq. (2) x_1 term (pulse frequency) appears only in the denominator part as linear term. This suggests that pulse frequency has inverse effect or inferior effect on MRR. x_4 term (pulse energy) appears both in the numerator and denominator part. This gives a hint that its effect on MRR is both increasing and decreasing. Also, it can be seen from Eq. (1) for Kw that interaction terms exist in the model developed based on GP. Conclusions for other parameters may be similarly drawn. It should be noted that the algorithm is able to ascertain between the relevant and

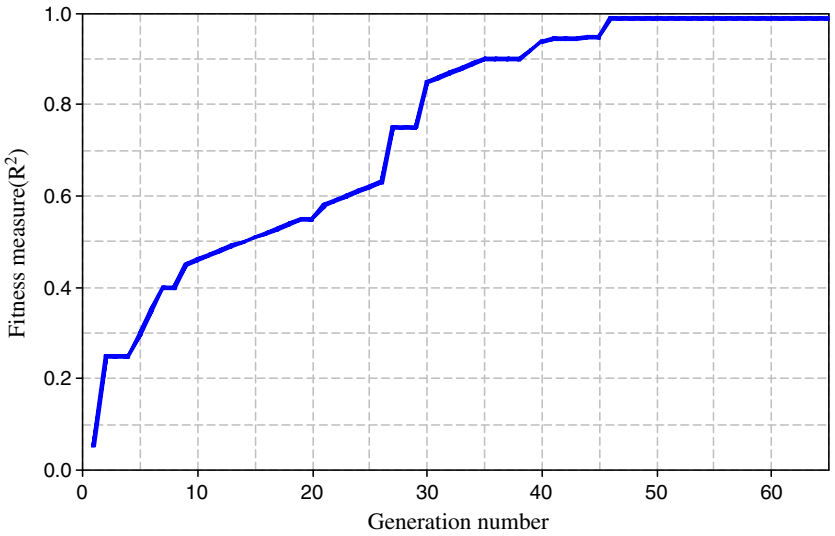

Fig. 5 Convergence plot of Kw model

irrelevant input data, evolving parsimonious system representation. The detailed direct effects and surface plots of process parameters for both the outputs Kw and MRR are discussed in the following sections.

7.5 Effect of process parameters on kerf width

7.5.1 Direct effects

As shown in Fig. 11a at low pulse frequency, there is enough time between the pulses for the material to substantially cool down. This helps extinguish the exothermic oxidation reaction thereby reducing the overall process efficiency. Furthermore as the material cools down between pulses at low pulse frequencies, there is greater likelihood of forming dross. The resulting lower average temperature increases the surface tension or viscosity of the molten material making it more difficult to flow out of the reaction zone, thus increasing the kerf. The kerf width varies from lower to higher values as shown in Fig. 11b due to different material removal mechanisms. At lower levels of pulse width due to lower pulse-to-pulse overlap, individual laser pulses affect the kerf. The average kef width generally decreases with increasing the cutting speed as shown in Fig. 11c. The faster the cutting, the smaller the energy density supplied to the material and lesser time there is for the heat to diffuse sideways and hence the narrower the kerf. Due to small workpiece thickness, no significant variation in kerf width is detected. Figure 11d shows that an increase of energy input per unit length lead to an increase in kerf width. The minimum value for the kerf width is obtained for the lowest energy input per unit length, and exceeding this value results in an increase in kerf width. An increase of laser energy normally leads to reduction of cut quality,

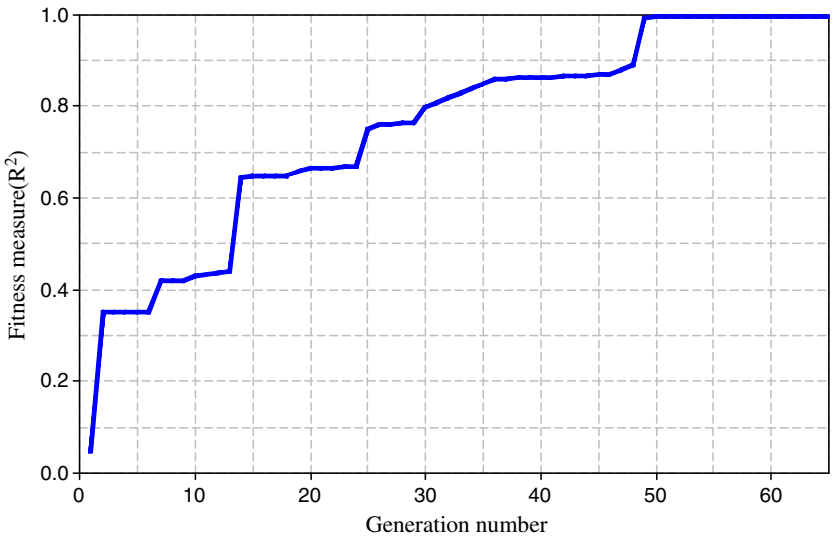

Fig. 6 Convergence plot of MRR model

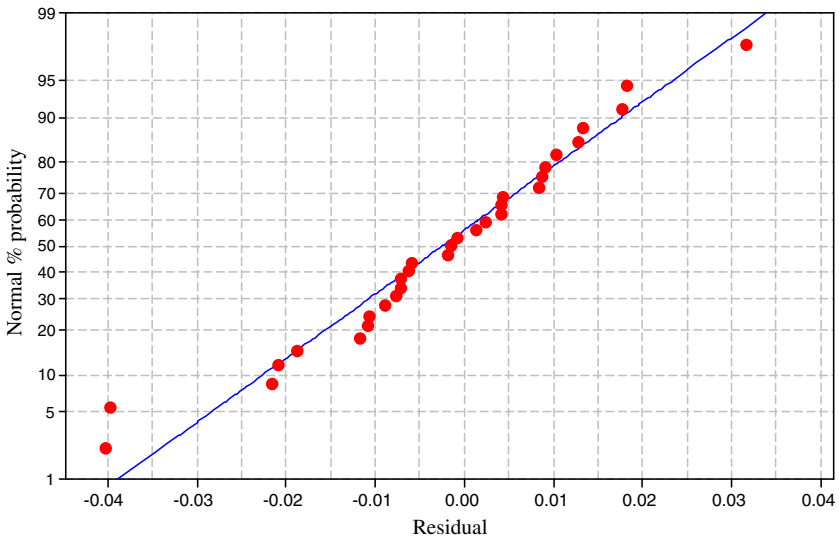

Fig. 7 Normal probability plot of residuals for Kw

consequently higher kerf widths result. At higher range if gas pressure is not increased, more molten material is ejected towards the top of the interaction zone and is melting additional material resulting in large kerf. The average cut width increases as the laser cutting energy increases. Low pulse energy leads to small thickness of recast layer and additionally causes low kerf width.

7.5.2 Surface plots

Figure 12 shows the 3D surface plots for kerf width. In Fig. 12a, the pulse width and cutting speed values are kept constant at 0.60 ms and 700 mm/min. An increase in pulse energy and pulse frequency results in higher kerf width. However the effect of changing pulse energy on kerf width is more dominant than pulse frequency. At high pulse energy and frequency, the intense melting, vaporization coupled with exothermic reaction of reaction gas, produces a kerf width of wide disorder. At low pulse frequency and pulse energy, the cutting process is more consistent and results in low kerf width. The effect of cutting speed and pulse width on kerf width is shown in Fig. 12b. It is evident that for lower pulse width, the kerf width gradually increases with increase in cutting speed and then decreases with decrease in cutting speed. At lower pulse width, the amount of energy supplied is limited, thus less amount of metal is displaced over the small area at low cutting speeds. Figure 12c shows the effect of pulse width and pulse energy on kerf width. Pulse width being the duration of laser pulse controls the incidental heat input into the part. At low values of pulse width and pulse energy, the variation in kerf width is minimal. At high value of pulse energy with subsequent increase in pulse energy, the variation is more phenomenal due to more material ejection. As the pulse width and pulse

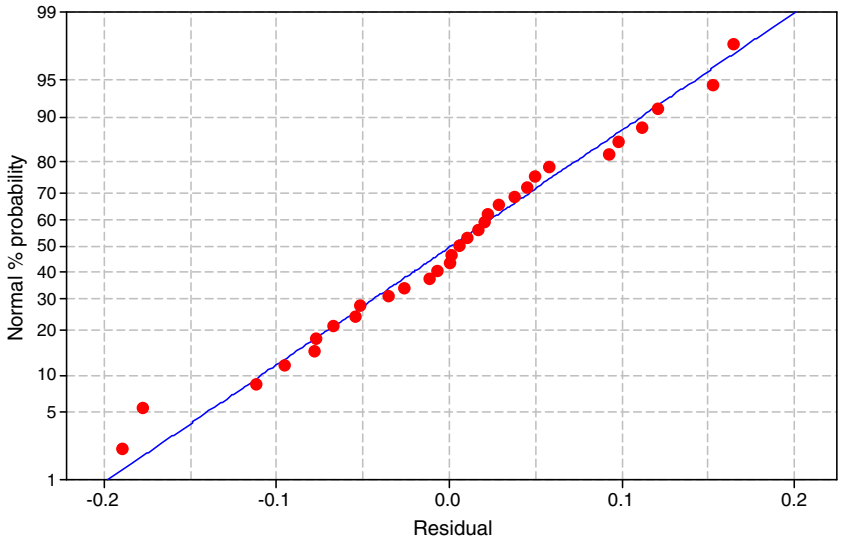

Fig. 8 Normal probability plot of residuals for MRR

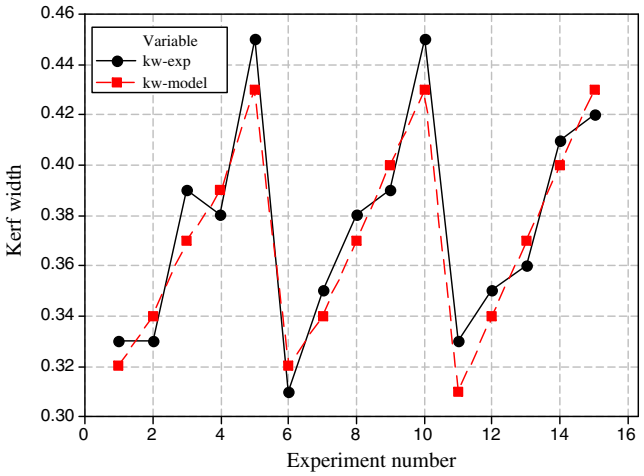

Fig. 9 Comparison of predicted values and experimental values of validation dataset for Kw

energy increase, they cause more metal removal which increases the kerf width. Figure 12d shows the effects of cutting speed and pulse energy on the kerf width, keeping pulse frequency and pulse width at 175.5 Hz and 0.6 ms. The plot reveals that cutting speed has nonlinear effect on kerf width at different pulse energy values. At lower value of cutting speed, the variation of kerf width with pulse energy is less, but at higher values the variation is significant. The kerf width varies almost linearly wrt pulse energy. Initially when the cutting speed and pulse energy are low, the melting and vaporization of work material are more stable. At higher cutting speeds and low energy levels, there is less time for heat diffusion and melting and hence low kerf width. Low cutting speeds and high pulse energy make the heat input to be concentrated for a longer period causing a large area to be removed from the surface, and hence, significant increase in kerf width is obtained.

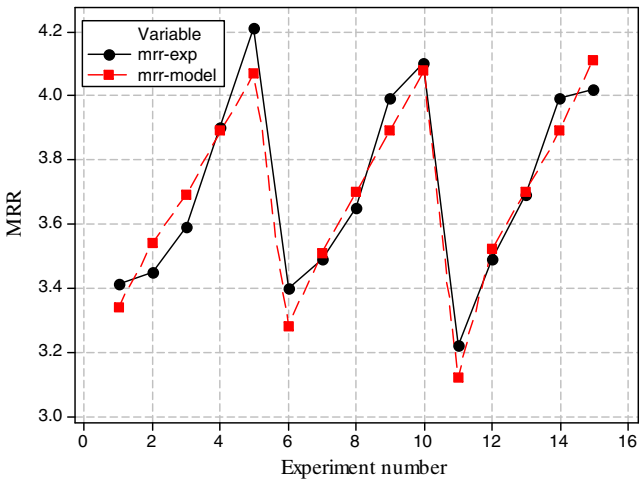

Fig. 10 Comparison of predicted values and experimental values of validation dataset for MRR

Table 6 Comparison of modelling results

	RSM			GP		
	Standard deviation	Mean absolute error	R^2	Standard deviation	Mean absolute error	R^2
Kw	0.042	0.061	0.950	0.033	0.017	0.999
MRR	0.392	0.165	0.976	0.287	0.068	0.998

7.6 Effect of process parameters on MRR

7.6.1 Direct effects

From Fig. 13a it is observed that as the laser repetition rate increases from minimum to maximum, material removal rate initially increases and then decreases. Each laser pulse acts in two stages: a melting stage where the temperature of the workpiece is raised to the vaporization temperature followed by a material removal stage where the vaporization occurs in a controlled manner. At low frequencies pulse irradiance level is high enough to reach vaporization temperature, hence material removal increases, but at high pulse frequency pulse irradiance is low and hence the vaporization temperature is not reached, so there is no vaporization resulting in low MRR. The effect is similar to pulse frequency as seen in Fig. 13b. At higher speeds laser energy is not sufficiently transferred to the interaction zone leading to low material interaction time and hence low MRR is seen as in Fig. 13c. Moreover due to small workpiece thickness, no significant variation in kerf width is detected. Figure 13d reveals there is a noticeable increase in MRR with an increase in pulse energy. As the pulse energy increases, each pulse cuts through the entire material and large portion of the material seems to be ejected at the bottom of the interaction zone. Also at higher energy levels, the ignition zone is expected to be wider because of the higher heat input as well as the limited thermal conductivity of the material.

7.6.2 Surface plots

Figure 14 shows the 3D surface plots for MRR. Figure 14a exhibits the variation of MRR with pulse frequency and pulse energy, while pulse width and cutting speed are fixed at 0.6 and 700. At low values of pulse frequency and pulse energy, the thermal energy incident on material is of small magnitude resulting in low MRR. Keeping frequency at low level, the increase in pulse energy causes significant improvement of material removal. But at high pulse frequency, as pulse energy of laser is lower, the amount of variation in MRR due to increase in pulse energy is comparatively lower. Increased pulse energy at low pulse frequency increases the incident thermal energy resulting in substantial material removal. Figure 14b shows the variation effect of

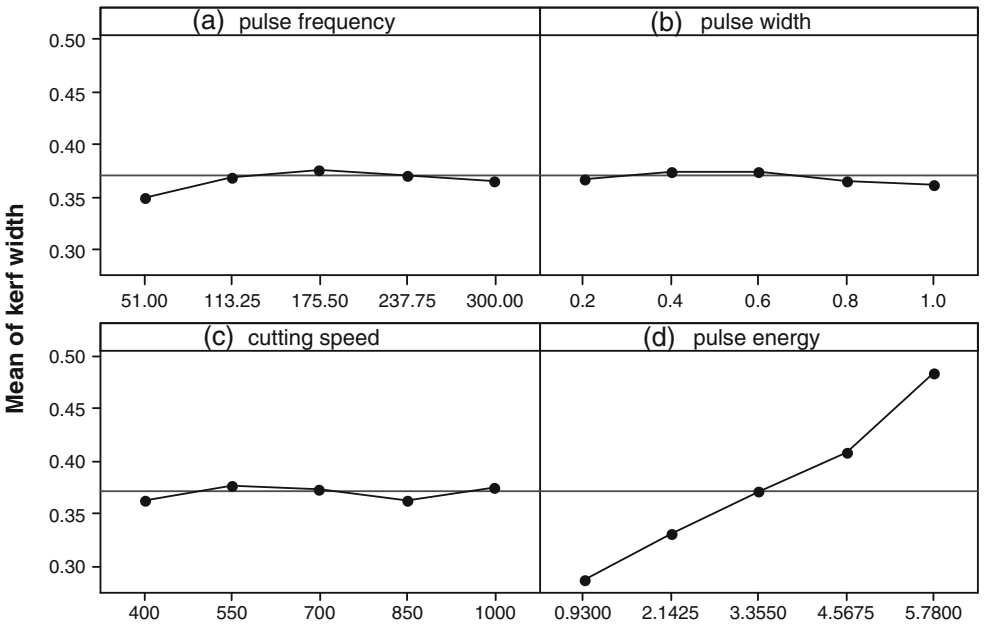

Fig. 11 Direct effects of process parameters on Kw. **a** Pulse frequency, **b** pulse width, **c** cutting speed and **d** pulse energy

pulse width and cutting speed on MRR, keeping pulse energy and pulse frequency constant at 3.355 and 175.5, respectively. The surface plot reflects the nonlinear variation of MRR with both the pulse width as well as cutting speed at different values. But MRR is highest at low levels of pulse width and cutting speed. Because of low pulse width and low cutting speed, the laser beam heat input is totally utilized to melt the material causing high MRR. Figure 14c shows the variation of MRR with pulse width and pulse energy while keeping the pulse frequency and cutting speed constant at 175.5 Hz and 700 mm/min, respectively. At low value of pulse width, low input laser beam energy results in small MRR. But at the same low range of pulse width, the MRR increases rapidly with pulse energy as high input energy of incident laser beam results in intense

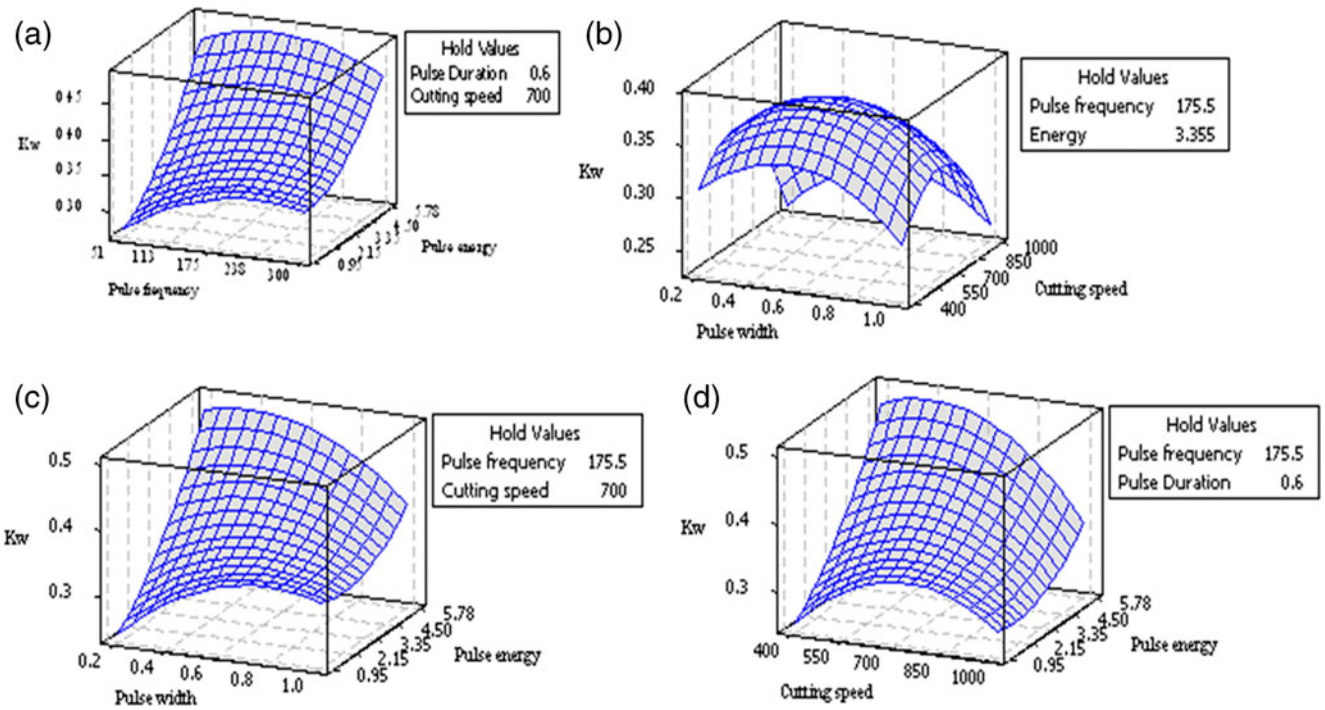

Fig. 12 **a**–**d** Surface plots of Kerf width

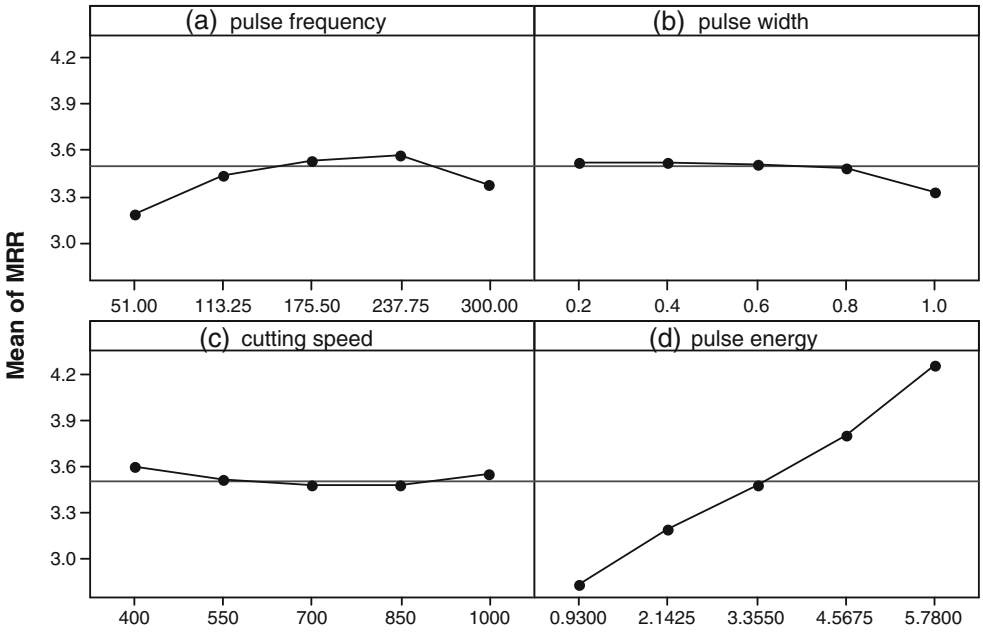

Fig. 13 Direct effects of process parameters on MRR. **a** Pulse frequency, **b** pulse width, **c** cutting speed and **d** pulse energy

melting and vaporization along the complete thickness of material. Figure 14d shows the effect of cutting speed and pulse energy on MRR by holding the pulse frequency and pulse width at 175.5 Hz and 0.6 ms. At lower values of pulse energy, the MRR varies parabolically wrt to increase in cutting speed. This may be attributed to the less heat input into the material at increasing speeds. The MRR holds a high value when the pulse energy is high and cutting speed is at a mid-value. High pulse energy generates high thermal energy resulting in improved MRR.

It is evident from Figs. 11, 12, 13 and 14 that among the chosen four control factors, pulse energy has profound effect on both the responses, whereas the effects of pulse width and cutting speed are found to be less significant.

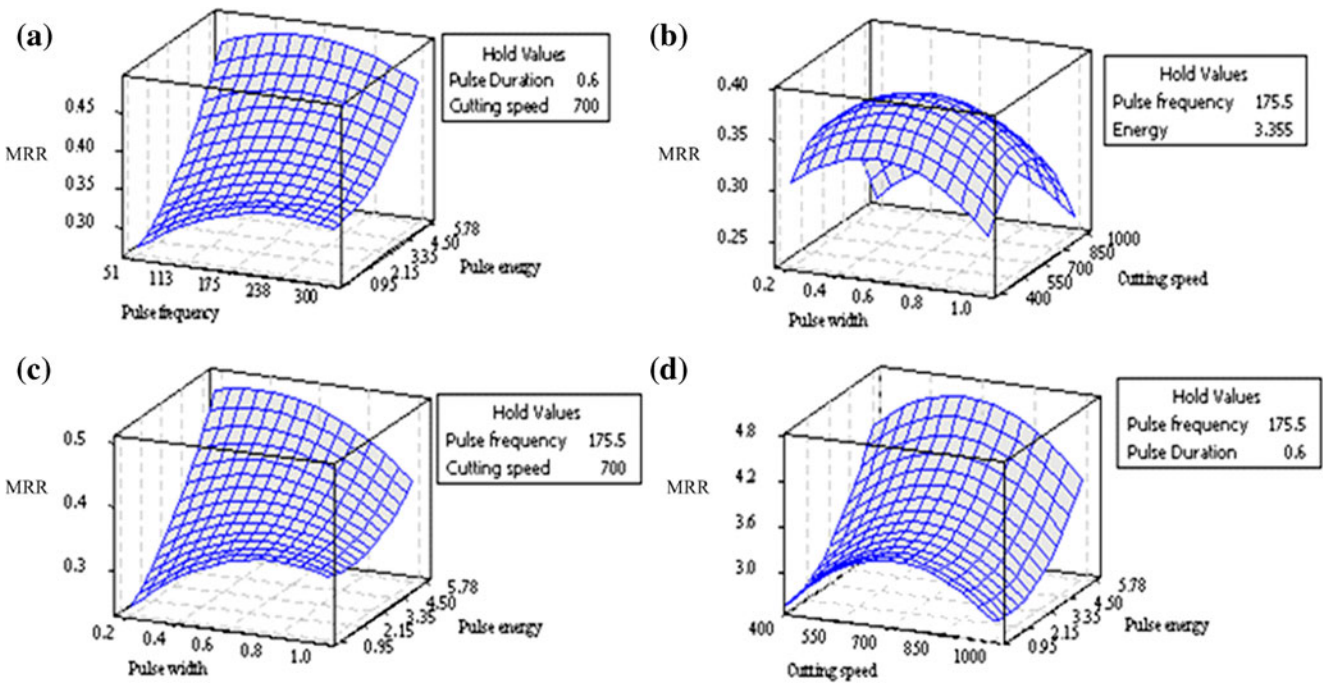

Fig. 14 **a**–**d** Surface plots of MRR

8 Formulation of multi-objective optimization problem

The two objective functions of the present study are:

1. Minimization of kerf width and
2. Maximization of material removal rate.

These are given by Eqs. (1) and (2), respectively. The two objective functions are optimized subject to the feasible bounds of input variables. The optimization problem is defined as follows:

Objective 1:Minimize

$$\mathrm{Kw} = \frac{(28.07 + x_4) - \left(\frac{x_3(0.09x_4 - x_2 + 29.38)}{(4.40 + 242x_3 - x_2x_3)}\right)}{(92 - x_4) + \left(\frac{23(x_2 - x_4)}{8.95 - x_2}\right) - \left(\frac{0.38}{x_1x_4}\right)} \tag{5}$$

Objective 2:Maximize

$$\mathrm{MRR} = \left(3 + 0.239(x_4 - x_2) + \frac{x_4}{x_1}\right) - \left(0.01x_3 - \frac{39}{x_1}\right) \times \left(\frac{5(19x_2 + 1604.17)}{(x_3 - 95(x_4 - x_1))(16 + x_4)}\right) \tag{6}$$

Subject to:

$$51\ \mathrm{Hz} \le x_1 \le 300.27\ \mathrm{Hz}$$

$$0.20\ \mathrm{ms} \le x_2 \le 1.0\ \mathrm{ms}$$

$$400\mathrm{mm/min} \le x_3 \le 1{,}000\ \mathrm{mm/min}$$

$$0.93\ \mathrm{J} \le x_4 \le 5.78\ \mathrm{J}$$

9 Results and discussions

The objective functions were optimized in compliance with the constraints given in Eqs. (5) and (6). As stated previously the NSGA-II algorithm was used for obtaining the Pareto

Table 7 Parameters for the NSGA-II algorithm

Population size (N)	50
Number of generations (N_{gen})	100
Crossover probability (P_c)	0.90
Mutation probability (P_m)	0.10
Distribution index for crossover operator (N_c)	20
Distribution index for mutation operator (N_m)	20

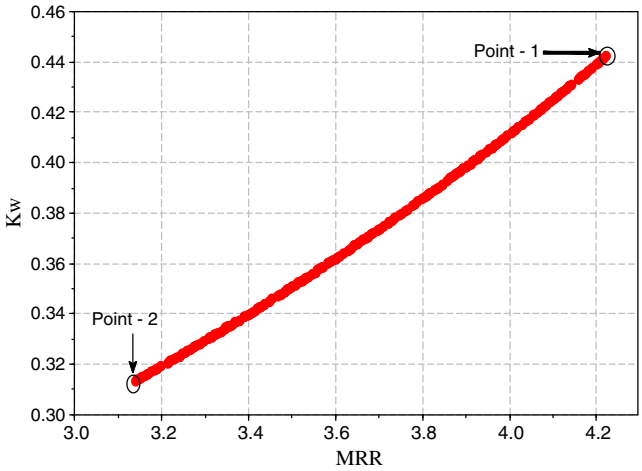

Fig. 15 Pareto optimal front

Table 8 Optimal values obtained through NSGA-II

S. no.	x_1 (Hz)	x_2 (ms)	x_3 (mm/min)	x_4 (J)	Kw (mm)	MRR (g/min)
1	224.37	0.72	677.42	1.28	0.314	2.992
2	290.03	0.33	580.54	4.40	0.405	3.902
3	207.01	0.31	902.28	4.47	0.408	3.834
4	172.85	0.46	799.30	2.62	0.351	3.320
5	263.84	0.62	775.29	5.53	0.442	4.073
6	250.35	0.86	587.90	4.81	0.415	4.264
7	252.24	0.23	713.83	4.46	0.408	3.910
8	201.25	0.29	752.12	2.60	0.352	3.394
9	274.43	0.43	500.45	3.46	0.316	3.656
10	180.01	0.75	650.15	5.52	0.441	4.026
11	190.18	0.62	572.80	5.24	0.432	4.010
12	137.15	0.32	736.62	2.34	0.345	3.257
13	177.00	0.48	773.16	2.77	0.315	3.365
14	247.22	0.57	484.64	1.88	0.330	3.227
15	195.47	0.31	542.86	1.54	0.312	3.154
16	257.30	0.23	450.65	5.44	0.442	4.196
17	147.01	0.70	646.10	5.71	0.448	4.063
18	191.28	0.61	407.20	3.78	0.384	3.685
19	260.39	0.27	940.64	3.48	0.377	3.621
20	118.16	0.62	460.38	5.28	0.433	4.005
21	240.03	0.31	494.94	3.71	0.384	3.738
22	208.20	0.20	685.02	4.34	0.404	3.870
23	165.12	0.34	883.84	5.67	0.449	4.098
24	226.79	0.54	458.77	4.38	0.403	3.851
25	174.56	0.24	689.51	1.45	0.322	3.106
24	271.22	0.78	517.12	5.71	0.448	4.122
27	208.14	0.25	605.40	5.47	0.442	4.220
28	298.90	0.73	993.66	1.12	0.310	2.930
29	274.43	0.43	500.45	3.46	0.376	3.656
30	267.69	0.31	561.78	3.19	0.369	3.606

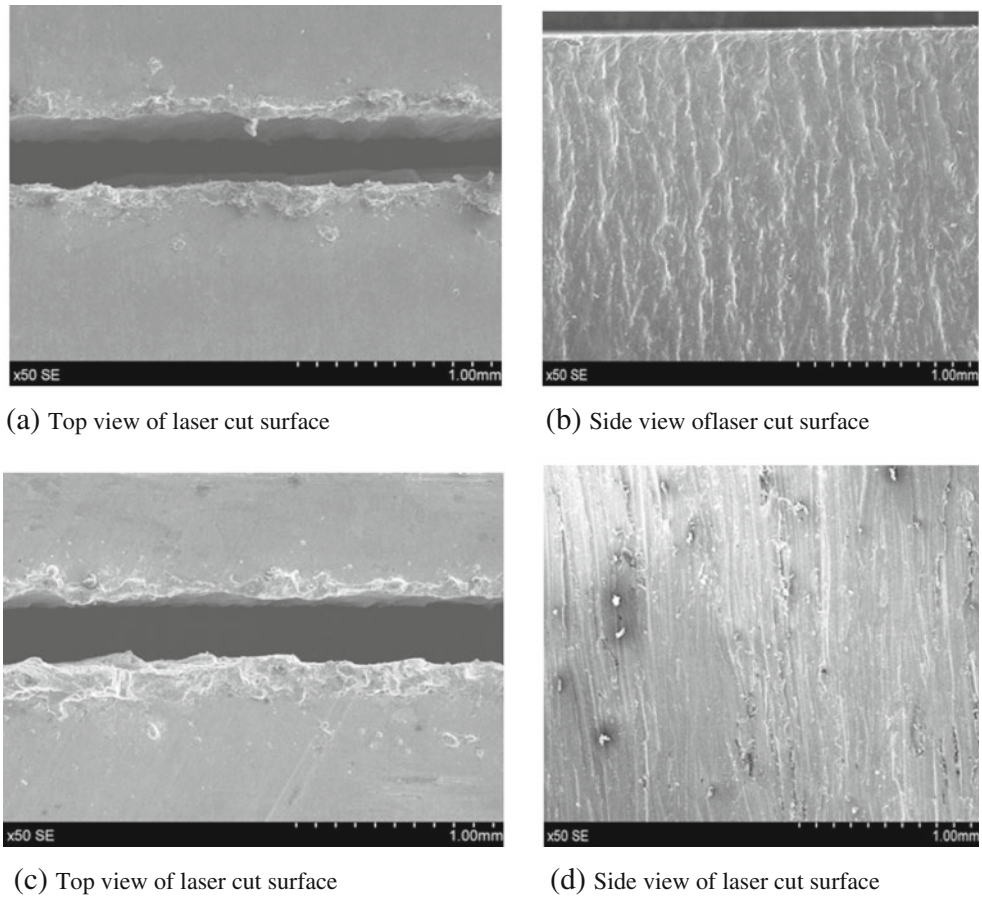

(a) Top view of laser cut surface

(b) Side view oflaser cut surface

(c) Top view of laser cut surface

(d) Side view of laser cut surface

Fig. 16 SEM photographs at the optimal values of individual output responses. **a** Top view of laser cut surface. **b** Side view of laser cut surface. **c** Top view of laser cut surface. **d** Side view of laser cut surface. x_1= 208.14 Hz, x_2=0.25 ms, x_3= 605.40 mm/min, x_4=5.47 J, Kw=0.442 mm, MRR= 4.220 m/min, x_1=195.47Hz, x_2=0.31 ms, x_3= 542.86mm/ min, x_4=1.54J, Kw=0.320mm, MRR=3.154gm/min

optimal solutions. The source code for NSGA-II is implemented in the VC++ programming language on Windows XP platform. The optimization results are sensitive to algorithm parameters, typical of heuristic techniques. Hence, it is required to perform repeated simulations to find commensurate values for the parameters. The best parameters for the NSGA-II, selected through 10 test simulation runs, are listed in Table 7. A population size of 100 was chosen with crossover probability of 0.90 and mutation probability of 0.10 along with other control parameters. NSGA-II gave good diversity results and provided for a well-populated Pareto front of the conflicting objective functions as shown in Fig. 15.

Among the 100 non-dominated optimal solutions at the end of 100 generations, 30 optimal input variables and their corresponding objective function values are presented in Table 8. By analysing the Pareto front, a decision maker can exploit it in accomplishing specific decisions based on the requirements of the process. For instance at point 1 in Fig. 15, laser cutting may be performed at maximum MRR but the Kw will be a higher value and hence poor edge quality. On the other extreme of the front, i.e. point 2 low Kw with good edge quality may be obtained but the MRR is minimum. All the other points on the front are in between cases. As can be observed from the graph, no solution in the front is absolutely better than any other as they are non-dominated solutions; hence, any one of them is an acceptable solution. The choice of a particular solution has to be made purely based on production requirements. For example if the manufacturer chooses to cut a component with Kw of 0.314 mm, the set of input variables may be selected from the first row of Table 8. Accordingly the MRR of 2.99 g/min would be achieved. In another instance from the experimental results of Table 3, 13th row, the set of input variables leads to MRR of 3.66 and the corresponding Kw value is 0.3985 mm. After optimization, the Kw value is reduced to 0.316 mm (S. no. 9, Table 8) with almost the same value of MRR.

The scanning electron microscopy (SEM) photographs of the samples that correspond to the best values of Kw and MRR are shown in Fig. 16a–d. Those values of Kw and MRR correspond to the extreme positions (point 1 and point 2) of the Pareto optimal set shown in Fig. 15. Both the top surfaces as well as the side view of laser cut surface are shown. As can be observed from the photographs, the variation of Kw and resultant striations is apparent with respect to the different optimal sets of input variables.

10 Conclusions

The laser cutting process is an important and widely used nontraditional manufacturing technology for rapid and precise cutting of metallic sheets with complex shapes yielding excellent accuracy and quality. Being a complex process, it is very difficult and costly to determine the optimal parameters based on trial and error or experience. The present work implements unique approach for laser cutting process based on the integration of two evolutionary approaches, namely GP and NSGA-II. GP is a powerful evolutionary modelling approach that can learn the complex underlying relationship between the input and response parameters effectively, whereas NSGA-II is reliable and widely established tool for multi-objective optimization.

In this work, the most important performances of laser cutting, namely MRR and kerf width, are considered. Initially, from the experimental training data, GP was used to model the mathematical relations for the chosen performance measures. Then, the models developed by GP were tested for their accuracy and suitability using statistical methods. The individual effects and the surface plots of the input variables on the chosen output parameters were also presented. Later, the validated mathematical models of GP were used by NSGA-II to find the multiple sets of optimal solutions so as to enable a manufacturing engineer to choose a particular optimal operating set of input variables according to the specific requirements. The selection of optimum values is essential for process automation and implementation of a computer-integrated manufacturing system.

References

1. Walsh RA, Cormier DR (2006) McGraw-Hill machining and metalworking handbook, 3rd edn. McGraw-Hill, New York
2. Prasad GVS, Siores E, Wong WCK (1998) Laser cutting of metallic coated sheet steels. J Mater Process Technol 74:234–242
3. Dubey AK, Yadava V (2008) Laser beam machining—a review. Int J Mach Tool Manuf 48:609–628
4. Yousef BF, George K, Knopf, Evgueni V, Bordatchev, Suwas K, Nikumb (2003) Neural network modeling and analysis of the material removal process during laser machining. Int J Adv Manuf Technol 22:41–53. doi:10.1007/s00170-002-1441-9
5. Li C-H, Tsaia M-J, Yang C-D (2007) Study of optimal laser parameters for cutting QFN packages by Taguchi's matrix method. Optic Laser Tech 39:786–795
6. Jimin C, Yang J, Zhang S, Zuo T, Guo D (2007) Parameter optimization of non-vertical laser cutting. Int J Adv Manuf Technol 33:469–473. doi:10.1007/s00170-006-0489-3
7. Dhara SK, Kuar AS, Mitra S (2008) An artificial neural network approach on parametric optimization of laser micro-machining of die-steel. Int J Adv Manuf Technol 39:39–46. doi:10.1007/s00170-007-1199-1
8. Dubey AK, Yadava V (2008) Multi-objective optimisation of laser beam cutting process. Optic Laser Tech 40(3):562–570
9. Avanish Kumar D, Vinod Y (2008) Optimization of kerf quality during pulsed laser cutting of aluminium alloy sheet. J Mater Process Technol 204(11):412–418
10. Ming-Jong T, Chen-Hao Li, Cheng-Che C (2008) Optimal laser-cutting parameters for QFN packages by utilizing artificial neural networks and genetic algorithm. J Mater Process Technol 208(1–3):270–283
11. Sardiñas RQ, Santana MR, Brindis EA (2006) Genetic algorithm based multi-objective optimization of cutting parameters in turning processes. Eng Appl Artif Intell 19:127–133
12. Deb K, Pratap A, Agarwal S, Meyarivan T (2002) A fast and elitist multiobjective genetic algorithm: NSGA-II. IEEE Trans Evol Comput 6(2):182–197
13. Koza JR (1992) Genetic programming: on the programming of computers by means of natural selection. MIT Press, Cambridge
14. Goldberg DE (1989) Genetic algorithms in search, optimisation, and machine learning. Addison-Wesley, Reading, MA
15. Dolinsky JU, Jenkinson ID, Colquhoun GJ (2007) Application of genetic programming to the calibration of industrial robots. Comput Ind 58:255–264
16. Zhang L, Jack LB, Nandi AK (2005) Fault detection using genetic programming. Mech Syst Signal Proc 19(2):271–289
17. Ashour AF, Alvarez LF, Toropov VV (2003) Empirical modelling of shear strength of RC deep beams by genetic programming. Comput Struct 81(5):331–338
18. Kondayya D, Gopalakrishna A (2010) An integrated evolutionary approach for modelling and optimization of wire electrical discharge machining. Proc IME B J Eng Manufact 225:549–567. doi:10.1243/09544054JEM1975
19. Poli R, Langdon WB, McPhee NF (2010) A field guide to genetic programming. http://www.gp-field-guide.org.uk. Accessed Dec 2010
20. Konak A, Coit DW, Smith AE (2006) Multi-objective optimization using genetic algorithms: a tutorial. Reliab Eng Syst Saf 91 (9):992–1007
21. Deb, K.; Agarwal, S.; Pratap, A.; Meyarivan, T (2000) A fast elitist nondominated sorting genetic algorithm for multiobjective optimization: NSGA II. In Proceedings of the Parallel Problem Solving from Nature VI (PPSN-VI), Springer: NY, 849–858
22. Deb K, Pratap A, Agarwal S, Meyarivan T (2002) A fast and elitist multiobjective genetic algorithm: NSGA-II. IEEE Trans Evol Comput 6(2):182–197
23. Banzhaf W, Nordin P, Keller R, Francone F (1998) Genetic programming: an introduction. Morgan Kaufmann, San Francisco
24. Koza JR, Bennett FH III, Andre D, Martin A, Keane (1999) Genetic programming III: Darwinian invention and problem solving. Morgan Kaufmann, San Francisco